AIP Journal of Applied Physics

Phase control of Mn-based spinel films via pulsed laser deposition

Zhenxing Feng, Xiao Chen, Timothy T. Fister, Michael J. Bedzyk, and Paul Fenter

Citation: Journal of Applied Physics **120**, 015307 (2016); doi: 10.1063/1.4955135
View online: http://dx.doi.org/10.1063/1.4955135
View Table of Contents: http://scitation.aip.org/content/aip/journal/jap/120/1?ver=pdfcov
Published by the AIP Publishing

JOURNAL OF APPLIED PHYSICS **120**, 015307 (2016)

Phase control of Mn-based spinel films via pulsed laser deposition

Zhenxing Feng,[1,2,a)] Xiao Chen,[3] Timothy T. Fister,[1,2] Michael J. Bedzyk,[3,4] and Paul Fenter[1,2,a)]
[1]*Chemical Science and Engineering Division, Argonne National Laboratory, Lemont, Illinois 60439, USA*
[2]*Joint Center for Energy Storage Research, Argonne National Laboratory, Lemont, Illinois 60439, USA*
[3]*Applied Physics Program, Northwestern University, Evanston, Illinois 60208, USA*
[4]*Department of Materials Science and Engineering, Northwestern University, Evanston, Illinois 60208, USA*

(Received 19 February 2016; accepted 18 June 2016; published online 6 July 2016)

Phase transformations in battery cathode materials during electrochemical-insertion reactions lead to capacity fading and low cycle life. One solution is to keep the same phase of cathode materials during cation insertion-extraction processes. Here, we demonstrate a novel strategy to control the phase and composition of Mn-based spinel oxides for magnesium-ion battery applications through the growth of thin films on lattice-matched substrates using pulsed laser deposition. Materials at two extreme conditions are considered: fully discharged cathode $MgMn_2O_4$ and fully charged cathode Mn_2O_4. The tetragonal $MgMn_2O_4$ (MMO) phase is obtained on $MgAl_2O_4$ substrates, while the cubic MMO phase is obtained on MgO substrates. Similarly, growth of the empty Mn_2O_4 spinel in the cubic phase is obtained on an MgO substrate. These results demonstrate the ability to control separately the phase of spinel thin films (e.g., tetragonal vs. cubic MMO) at nominally fixed composition, and to maintain a fixed (cubic) phase while varying its composition ($Mg_xMn_2O_4$, for $x = 0, 1$). This capability provides a novel route to gain insights into the operation of battery electrodes for energy storage applications. *Published by AIP Publishing.* [http://dx.doi.org/10.1063/1.4955135]

I. INTRODUCTION

Spinel oxides, AB_2O_4, are widely used as catalysts,[1,2] magnetic and ferroelectric devices,[3,4] and as cathodes for lithium ion (e.g., $Li_xMn_2O_4$)[5] and multivalent ion batteries (Mg^{2+}, Al^{3+}, etc., compared to Li^+).[6,7] Attractive properties include their low cost, low toxicity, and thermal stability.[8] Li-based spinel cathodes operate only within a limited lithium composition range: λ-$Mn_2O_4 \leftrightarrow Li_xMn_2O_4$ for $0 \leq x \leq 1$, corresponding to a maximum charge capacity of ~140 mA h/g.[5] This capacity limitation is associated with the occurrence of a structural phase change that occurs for $x > 1$, at which point $Li_xMn_2O_4$ (LMO) begins to transform from a cubic to a tetragonal phase.[9] This structural change is associated with instabilities in LMO cathode, leading to capacity loss upon extended cycling. A similar issue was found for spinel-based Mg-cathodes: the insertion of Mg^{2+} into λ-MnO_2 leads to a phase transformation from the cubic to tetragonal phase of $MgMn_2O_4$ (MMO).[7] It is therefore expected that the phase stabilization of the cathode during cation insertion/extraction may be beneficial in the development of battery cathodes with high energy density and long cycle life.

It is difficult to maintain phase stability of powder materials under electrochemical charging/discharging conditions. For example, the empty (i.e., fully charged) cathode MnO_2 has several structural phases, such as α-MnO_2 (tetragonal I4/m; $a = b = 9.777$ Å and $c = 2.855$ Å),[10] β-MnO_2 (tetragonal $P4_2$/mnm; $a = b = 4.398$ Å and $c = 2.873$ Å),[11,12] ε-MnO_2 (hexagonal $P6_3$/mmc; $a = b = 2.80$ Å and $c = 4.45$ Å),[13] γ-MnO_2 (orthorhombic Pnma; $a = 4.45$ Å, $b = 9.305$ Å, and $c = 2.85$ Å),[14] and λ-MnO_2 (or spinel Mn_2O_4, cubic $Fd\bar{3}m$; $a = 8.029$ Å).[15] Although at room temperature the magnesiated (i.e., discharged) cathode, MMO, adopts a tetragonal spinel structure in space group $I4_1$/amd with $a = b = 5.727$ Å and $c = 9.284$ Å,[16] it adopts a cubic phase in space group $Fd\bar{3}m$ with $a = 8.600$ Å at high temperature (>950 °C)[16,17] or high pressure (>15.6 GPa).[18] To minimize the complexity associated with phase changes in powder-based electrodes, we chose, instead, to study epitaxial thin films, as many parameters such as geometry, orientation, and surface termination can be controlled rationally. Epitaxial thin films often follow the structures of the underlying substrates, and the relative stability of different phases can be controlled through the use of lattice strain.[19,20]

Herein, we demonstrate the growth and phase-control of the spinel MMO as epitaxial thin films for advanced battery cathode applications using pulsed laser deposition (PLD). PLD enables the growth of hetero-structured thin films with sharp interfaces and atomically smooth surfaces[20] and enables the growth of metastable crystalline structures,[21,22] allowing for the exploration of new materials with different properties and novel functionalities. Specifically, we demonstrate the phase-selective growth of high quality MMO thin films with either cubic or tetragonal phases by choosing different substrates, namely, MgO (cubic $Fm\bar{3}m$, $a = 4.212$ Å) vs. $MgAl_2O_4$ (MAO, cubic $Fd\bar{3}m$, $a = 8.083$ Å) and growth conditions (e.g., substrate temperature, gas pressure, and laser power). In addition, we also demonstrate the ability to control the composition of the cubic spinel by growing the empty spinel phase, Mn_2O_4, on an MgO substrate. This independent control of spinel phase (cubic vs. tetragonal) and composition (empty vs. Mg-containing) at room temperature and ambient condition introduces a new potential route for

---

[a)]Authors to whom correspondence should be addressed. Electronic addresses: fengz@anl.gov and fenter@anl.gov synthesizing battery cathodes with intrinsically higher stability.

II. EXPERIMENTAL DETAILS

Epitaxial $Mg_xMn_2O_4$ ($x \approx 0, 1$) films were prepared by PLD on polished single crystal substrates, having a size of $5 \times 5 \times 1\,mm^3$ MgO(001) (from MTI Corporation) or MAO(001) (from CrysTec). The MMO target with 25 mm diameter was synthesized using solid-state methods from stoichiometric mixtures of MgO and Mn_2O_3 (Alfa Aesar, USA) powders and was calcined at 1100 °C in air for 72 h. At room temperature (25 °C) and ambient pressure (1 atm or 101 kPa), the MMO target exhibits the expected tetragonal phase (Figure S1[23]). The MnO_2 target (Figure S2[23]) was prepared using β-MnO_2 sintered at 1100 °C in air for 72 h. The MgO substrates were annealed in air at 1000 °C for 10 h to obtain atomically flat surfaces (Figure S3[23]). PLD was performed using a KrF excimer laser ($\lambda = 248$ nm) at 500 °C under 10 mTorr O_2 for 2500 pulses (~10 nm) and 7500 pulses (~30 nm) on MgO(001) and 1500 pulses (~5 nm) on $MgAl_2O_4$(001). In addition, 10 000 pulses (~40 nm) of Mn_2O_4 were grown on MgO(001) at 650 °C under 10 mTorr O_2. Reflection high-energy electron diffraction (RHEED) was utilized for diagnostic *in situ* monitoring of the film growth. RHEED oscillations (Figure S4[23]) were observed during MMO growth, indicating the layer-by-layer growth. The surface morphology of MMO films was examined by atomic-force microscopy (AFM, Veeco Nanoscope IV).

Thin film X-ray diffraction (XRD) was performed using a four-circle diffractometer (X'Pert PRO, PANalytical) in specular and off-specular configurations with Cu Kα_1 ($\lambda = 1.5406$ Å) radiation. Further characterization was performed with X-ray reflectivity (XRR) at sector 33 BM of the Advanced Photon Source (APS) in Argonne National Laboratory (ANL) using 20 keV X-rays with a beam size of 2.0 mm horizontally and 0.1 mm vertically and an incident flux of $\sim 10^{10}$ photons per second. Scattered X-rays were detected using a pixel array detector (Dectris PILATUS 100K). The sample was placed in a custom-designed chamber and purged with helium during the XRR measurement to avoid oxidization related to ozone generation from intense X-ray beam. Low-angle XRR and specular (00L) crystal truncation rod (CTR) measurements were performed on both MMO/MgO and MMO/MAO films, and off-specular (11L) CTRs were carried out on MMO/MAO films only. The background and diffuse X-ray scattering contributions in CTR were subtracted by selection of regions of interest of the area detector images. The final intensities were normalized and corrected taking into account beam polarization and Lorentz factors.

X-ray photoelectron spectroscopy (XPS) spectra (Thermo Scientific ESCALAB 250Xi) were collected at the Keck II facility of NUANCE at Northwestern University using monochromated Al Kα X-rays. A low-energy electron flood gun was used to compensate for XPS induced surface charging. The carbon 1s line (284.8 eV) was used as a reference to calibrate the XPS spectra. The depth-dependent composition was obtained after the samples were Ar-etched for depths up to 4–5 nm and analyzed by XPS.

III. RESULTS AND DISCUSSION

AFM analysis (Figure 1) reveals that MMO films on both MAO(001) and MgO(001), and Mn_2O_4 film on MgO(001) have atomically smooth surfaces, with root-mean-square (RMS) roughness ~2 Å. The original terraces from MgO substrates (Figure S2) are still visible after MMO and Mn_2O_4 growth, indicating a layer-by-layer growth mode, which is further supported by RHEED data collected during film growth (Figure S3[23]).

The thin film epitaxial relationship can be seen from *in situ* RHEED pattern (Figure 2). The MMO thin film RHEED patterns along the MgO[100] (Figure 2(c)) and MgO[110] (Figure 2(d)) directions are aligned with original MgO patterns (Figures 2(a) and 2(b)), indicating epitaxial growth. In addition, the RHEED patterns after MMO growth appear as rods of intensity instead of as spots, suggesting very smooth (RMS around several Å) thin film surfaces, consistent with AFM measurements. Note that MMO RHEED patterns have double the truncation rod density compared to MgO patterns, indicating that the MMO in-plane lattice constant is twice as

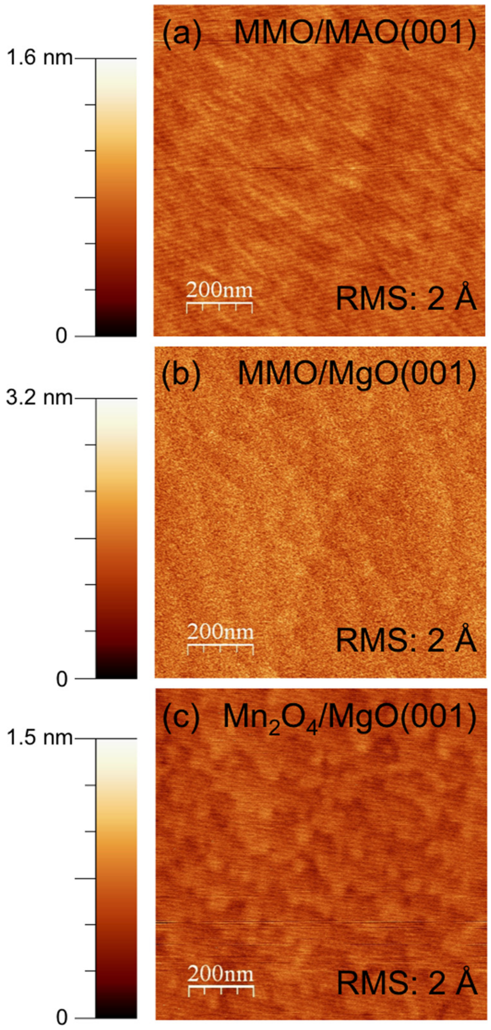

FIG. 1. $1 \times 1\,\mu m^2$ AFM image of (a) 5 nm $MgMn_2O_4$ film on $MgAl_2O_4$(001) (MMO/MAO) (001), (b) 10 nm MMO film on MgO(001), and (c) 30 nm Mn_2O_4 film on MgO(001). The atomic terraces originally from MgO(001) substrate are still visible after the film growth, indicating conformal layer-by-layer growth mode from PLD.

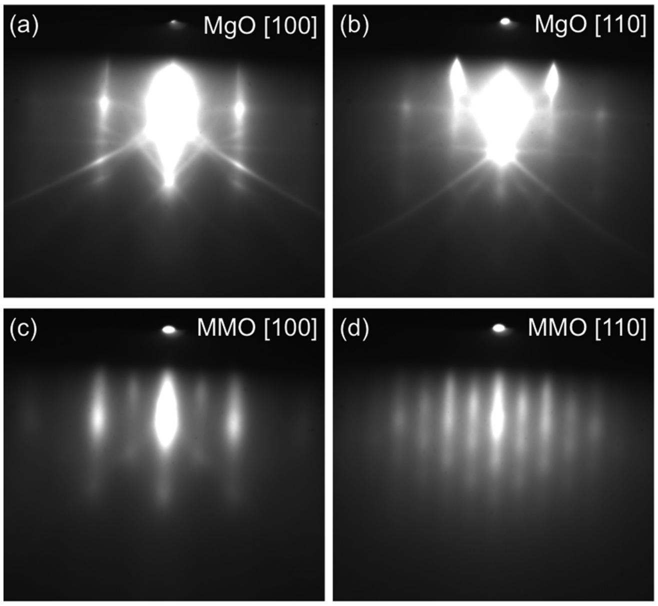

FIG. 2. Reflection high-energy electron diffraction (RHEED) patterns taken along the [100] and [110] azimuthal directions for (a) MgO [100], (b) MgO [110], (c) $MgMn_2O_4$ (MMO) [100], and (d) MMO [110]. Spinel patterns with in-plane lattice constants that are twice as large as those of the MgO substrate can be seen after MMO growth.

large as that of MgO. Similar RHEED patterns were observed for the epitaxial MMO/MAO (Figure S5[23]) and Mn_2O_4/MgO (Figure S6[23]) films.

The film structure and morphology was obtained with XRR. The XRR experimental data and model fits (Figure 3) are shown for samples with 1500 PLD pulses of MMO/MAO(001) and 2500 pulses of MMO/MgO(001) films. The data are plotted as a function of the vertical momentum transfer vector magnitude, $q = 4\pi \sin(2\theta/2)/\lambda$, where 2θ is the scattering angle and λ is the X-ray wavelength. The presence of oscillations extending to $q > 0.8\ \mathrm{A}^{\circ -1}$ indicates smooth, uniform film layers, which is consistent with AFM and *in situ* RHEED analysis. The XRR data were fitted by a three-layer model, which consists of a semi-infinite substrate crystal (MAO or MgO), an MMO bulk layer, a transition layer, and a lower density surface overlayer (Figure 3, inset). This low-density surface overlayer could be due to incomplete coverage from PLD growth. This analysis reveals film thicknesses of 54 ± 9 Å for MMO/MAO(001), and 102 ± 9 Å for MMO/MgO(001) with electron densities that are within 5% of the expected value. Comparing the laser pulses used for each film, these results suggest that MMO was deposited at approximately the same rate, 0.04 Å/pulse, on both MAO and MgO substrates. The surface roughness of the MMO film from XRR analysis is ∼2 Å, which is consistent with AFM results. Furthermore, the derived electron density profiles show that MMO films have a bulk-like density on both substrates, but with an additional ∼20 Å-thick surface overlayer having a density that is ∼25%–45% less than that expected for the MMO film (see Table S1 for detailed fitting values[23]). This might be due to the partially covered surface during PLD growth. Further analysis by depth-dependent XPS shows that the surface (∼1.5 nm in depth) is rich in carbon and oxygen, thus reducing the average film density at the top, consistent with the formation of adventitious carbon layer. In contrast, the "bulk" (deeper than 1.5 nm) compositions are roughly close to the nominal values, namely, $Mg_{1.05}Mn_2O_{3.98}$/MAO and $Mg_{0.94}Mn_2O_{4.05}$/MgO. This slight off-stoichiometry could introduce point defects to alter the film lattice constants.

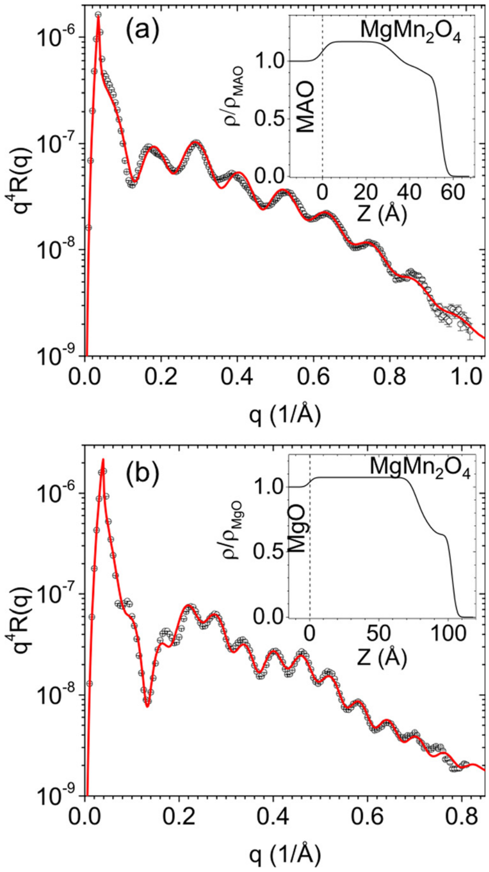

FIG. 3. X-ray reflectivity data (black dots) and fits (red lines) for (a) 1500 PLD pulses of MMO on MAO(001) and (b) 2500 PLD pulses of MMO on MgO(001). Insets in each figure show the electron density depth profiles obtained from XRR fits normalized to the electron density of the substrate. The corresponding model parameters are listed in Table S1 in supplementary material.

Epitaxial relationships between the MMO film and the MAO(001) substrate are further revealed in Figure 4. Specular (00L) CTR data (Figure 4(a)) for tetragonal MMO (MMO_T) grown on MAO(001) show that the film has its *c* axis aligned with the substrate *c* axis. The off-specular (11L) CTR in Figure 4(b) indicates the following alignment: MMO_T[101]//MAO[111]. This also implies that the MMO_T film unit cell has a 45° in-plane rotation with respect to MAO substrate unit cell, which is further supported by in-plane ϕ scan (Figure S7[23]). A crystal model is drawn in Figure 3(c) to better illustrate the epitaxial relationship between MMO_T and MAO. This is not surprising as bulk MMO_T has an in-plane lattice constant $a_{MMO} = 5.727$ Å. To keep an epitaxial growth with minimum strain, a 45° in-plane rotation is necessary to match the substrate lattice constant $\sqrt{2} * a_{MMO} = 8.099 \sim 8.083 = a_{MAO}$. From the XRD data, the average unit cell parameters of the MMO film were determined to be $c = 9.167$ Å and $a = 5.675$ Å. Thus, there is compressive in-plane strain ($\varepsilon_{xx} = -0.91\%$) with respect to the bulk MMO_T lattice ($a = b = 5.727$ Å and $c = 9.284$ Å (Ref. 16)).

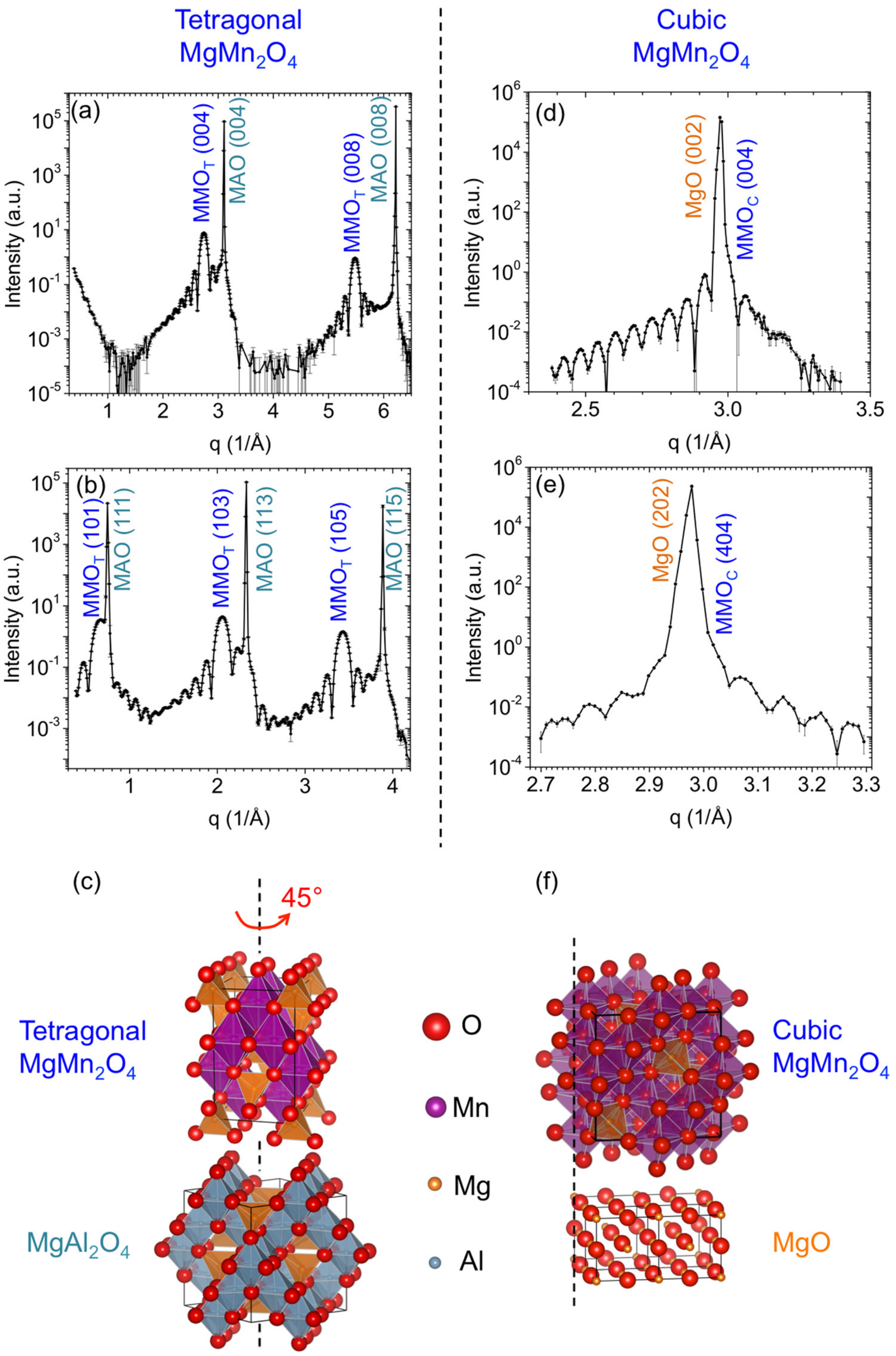

FIG. 4. Crystal truncation rod data along (a) specular (00L) and (b) off-specular (11L) for MMO$_T$/MAO(001). (d) Specular (00L) and (b) off-specular (20L) for MMO$_C$/MgO(001). (c) and (d) Schematic crystal models showing the observed epitaxial relationships for MMO$_T$/MAO(001) and MMO$_C$/MgO(001).

A surprising finding was the observation of the cubic phase of MMO (MMO$_C$) grown on MgO(001). Specular (00L) and off-specular (20L) CTR scans (Figures 4(d) and 4(e), respectively) of a 10 nm MMO film show clear thickness fringes around the MgO (002) and MgO (202) Bragg peaks, indicating the high quality and uniformity of the MMO$_C$ thin films grown from PLD. These also reveal the following cube-on-cube epitaxial relationships: MMO$_C$[001]//MgO[001] and MMO$_C$[404]//MgO[202]. Further evidence is from additional measurements at the substrate half-order peak locations. These half-order peaks are forbidden for MgO cubic phase but are allowed for the spinel cubic phase as the lattice constant of cubic spinel is approximately as twice as that of MgO. The representative MMO$_C$ only peaks (i.e., some substrate half-order peaks) can be found in Figure S8. Note that a long-range specular θ–2θ scan (Figure S9[23]) was also performed to check the potential presence of other phases. Neither peaks from MMO tetragonal phase nor other phases such as Mn$_2$O$_3$ (e.g., from the decomposition of MMO) were found. Similar experiments were conducted on 30 nm thick MMO films and the same cubic phase was found (Figure S10[23]). All these suggest that MMO films are preferentially grown in the cubic phase when grown on MgO(001) substrate via PLD (even using a MMO$_T$ target that has the tetragonal phase; Figure S1). Average lattice

TABLE I. Epitaxial relationship as well as bulk and thin film lattice constants of materials in this work. The in-plane strains are calculated using $\varepsilon_{xx} = {}^{(a_{film\_bulk} - a_{sub})}/_{a_{sub}}$, where a_{film_bulk} is the in-plane bulk lattice constant of the film material and a_{sub} is the substrate lattice constant of MgO or $MgAl_2O_4$ (MAO). For comparison, the last row lists the calculated in-plane strains if MMO_C were grown on MAO and MMO_T were grown on MgO. *R*45° denotes the in-plane 45° rotation. Here, we use 30 nm MMO_C and 54 nm MMO_T thin films as examples to illustrate the role of strain.

Materials	MgO	MMO_C	MAO	MMO_T
a_{Bulk}/c_{Bulk} (Å)	4.212	8.600	8.083	5.727/9.284
Epitaxy	...	Cube-on-cube	...	*R*45° in-plane
c_{Film} (Å)	...	8.384	...	9.167
a_{Film} (Å)	...	8.345	...	5.675
$\varepsilon_{xx} = {}^{(a_{film\_bulk} - a_{sub})}/_{a_{sub}}$	...	2.09% MMO_C/MgO	...	0.20% MMO_T/MAO
ε_{xx}	...	−3.86% MMO_T/MgO	...	6.40% MMO_C/MAO

constants were $c = 8.384$ Å and $a = 8.345$ Å for 30 nm MMO_C film, indicating a larger deviation from the bulk MMO_C lattices ($a = c = 8.600$ Å (Ref. 24)). The 10 nm MMO_C film is fully epitaxial with respect to the MgO substrate, namely, $a = 2{*}a_{MgO} = 8.424$ Å, indicating that the strain imposed from MgO substrate brings a closer match for the ultra thin film to the MMO_C bulk lattice spacing.

For MMO powders, the cubic phase is realized at temperatures above 950 °C (Refs. 16 and 17) or under a higher pressure ~15.6 GPa.[18] A possible cubic phase of an MMO thin film was recently suggested by sputtering deposition growth that showed a vertical coherence for the MMO thin film on an Al_2O_3 substrate.[25] The formation of highly epitaxial MMO_C/MgO and MMO_T/MAO could be related to strains imposed by the substrates. As shown in Table I, although MgO and MAO are both cubic phases, MgO has a lattice constant 4.212 Å, while MAO has a lattice constant 8.083 Å. Compared to the bulk lattice constants of 8.600 Å (Ref. 24) for MMO_C and 5.727 Å for MMO_T, the in-plane strain induced by MgO, $|(a_{MMO_C} - 2 * a_{MgO})/2 * a_{MgO}| = 2.09\%$, is less than the strain if MMO_T were grown on MgO, $|(\sqrt{2} * a_{MMO_T} - 2 * a_{MgO})/2 * a_{MgO}| = 3.86\%$. However, to grow MMO on MAO, the tetragonal phase has a great advantage due to the smaller in-plane strain, $(\sqrt{2} * a_{MMO_T} - a_{MAO})/a_{MAO} = 0.20\%$, as compared to that of MMO_C on MAO, $(a_{MMO_C} - a_{MAO})/a_{MAO} = 6.40\%$. Therefore, we conclude that strain is a dominant factor for controlling and stabilizing the different MMO phases as thin films. In particular, MgO substrate may provide the interaction that stabilizes the high T/P cubic MMO phase that has not previously been observed at ambient conditions.[16–18]

The cubic MMO film has quite different properties compared to its tetragonal phase. Previous work on powder materials has shown that MMO_C has an electrical resistivity of only ~10 Ω cm instead of ~10^6 Ω cm for the tetragonal phase,[17] which is beneficial for a battery electrode. In addition, tetragonal spinel oxides are known to have the distorted oxygen octahedra due to Mn(III) electronic configuration, t_{2g}^{3}-e_g^{1}, which induces the Jahn-Teller distortion.[26] This is believed to be the primary driving force for capacity fading in spinel materials such as $LiMn_2O_4$ as a lithium ion battery cathode. In particular, the tetragonal-to-cubic transition in MMO leads to a redistribution of Mg^{2+} into both tetrahedral and octahedral sites and will change the inversion degree of

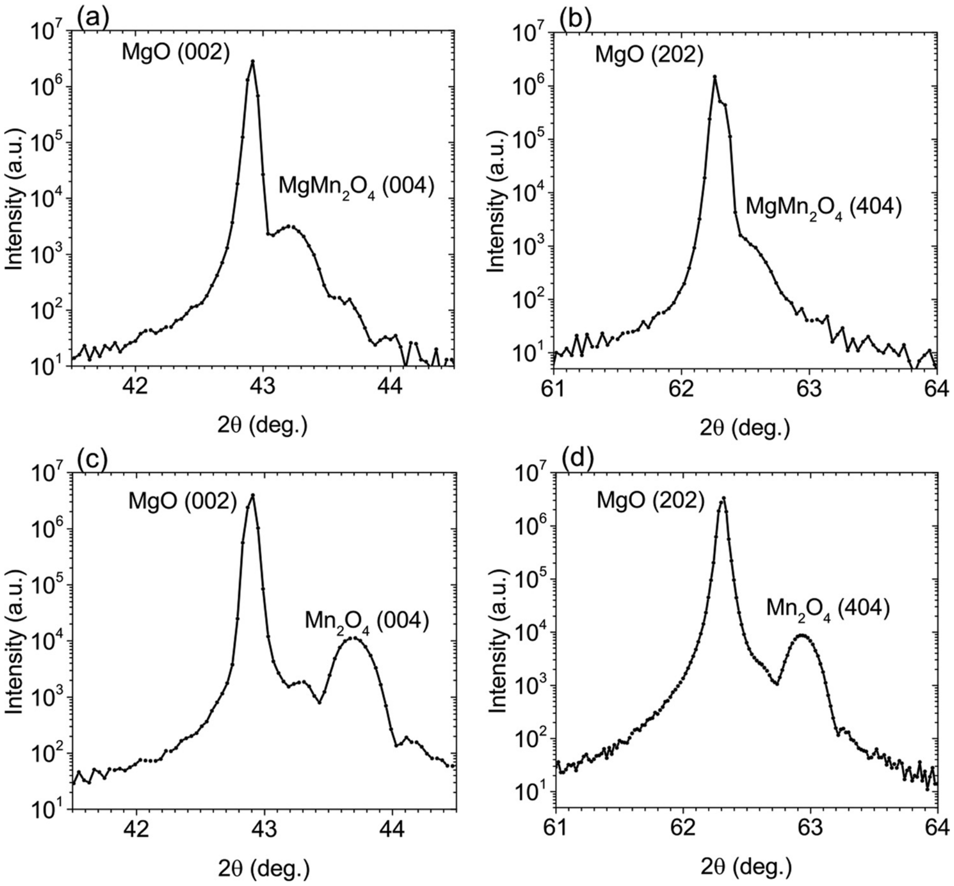

FIG. 5. Specular and off-specular X-ray diffraction data for thick (~20 nm) $MgMn_2O_4$ (MMO) and Mn_2O_4 grown on MgO (001) in the vicinity of (a), (c) MgO(002) and (b), (d) MgO(202), respectively. These suggest both MMO and Mn_2O_4 films are oriented by cubic-on-cubic epitaxy on MgO(001).

MMO_C from 0 to 0.45,[17] while Mg^{2+} only occupies the tetragonal sites in the tetragonal phase.[16,17]

These comparisons of MMO_C with respect to powder MMO indicate that MMO_C may be a good candidate as a model battery cathode. Although powder MMO_C cannot be obtained at room temperature and ambient pressure, the stabilized thin film MMO_C in this work might be utilized as a cathode in a thin film battery.[6,27] As cations in A site of spinel AB_2O_4 are extracted and inserted during battery cycling, it is also important to produce a stable A-site empty B_2O_4 (fully charged state) with the same phase as AB_2O_4 (discharged state). For this reason, Mn_2O_4 thin film was grown on MgO(001) and Figure 5 compares MMO_C (~30 nm) and Mn_2O_4 (~40 nm) grown on MgO(001). Results clearly show that the epitaxial Mn_2O_4 thin film is also cubic phase (see Figure S11 for more evidence). Note the cubic Mn_2O_4 is grown using a non-cubic phase of MnO_2 target (Figure S2). To the best of our knowledge, this is the first time where high quality epitaxial spinel Mn_2O_4 thin films were obtained in the cubic phase. The corresponding (004) and (404) peaks of Mn_2O_4 are at higher diffraction angles than those of MMO_C, indicating lattice constants of $c = 8.280$ Å and $a = 8.417$ Å. When compared to the lattice spacings of MMO_C ($c = 8.384$ Å and $a = 8.345$ Å), the c lattice spacing of Mn_2O_4 is smaller due to the shrinkage of the crystal lattice as a result of the empty A site, while a of Mn_2O_4 is closer to $2{*}a_{MgO} \sim 8.424$ Å, suggesting better in-plane coherence.

IV. CONCLUSION

In summary, we demonstrated the ability to synthesize phase-pure polymorphs of $MgMn_2O_4$ (MMO) thin films at room temperature and ambient pressure by PLD. The phase-selected growth of MMO thin films is controlled by the choice of substrate, with growth in the cubic phase (MMO_C) on MgO substrates and the tetragonal phase (MMO_T) on $MgAl_2O_4$ substrates. The ability to growth the Mn_2O_4 ($Mg_xMn_2O_4$ with $x = 0$) in cubic phase on MgO(001) (corresponding to a charged cathode) has also been established. As the MMO_C is a high temperature (>950 °C)[16,17] or high pressure (>15.6 GPa)[18] phase in the powder form, the formation of MMO_C as thin film at room temperature (25 °C) and ambient condition (101 kPa) is likely due to strains induced by the substrate host structure.

The controllable growth of stabilized tetragonal MMO_T phase as well as the cubic MMO_C and Mn_2O_4 phases opens up the use of these epitaxial thin film systems to understand the molecular-scale response of these materials to electrochemical reactions, as model cathodes for a multivalent battery system.[6] For example, the ability to grow the cubic phase of $Mg_xMn_2O_4$ at two compositional extremes ($x = 0$ and $x = 1$) using the substrate confinement method provides a novel system for understanding the relevant structures and interactions in model battery cathode interfaces. MMO can be used as a model for the discharged cathode relevant to a Mg battery,[28] while Mn_2O_4 represents the charged cathode for many battery chemistries (e.g., Li-, Zn-, Ca-batteries). Our recent work on MMO_C thin films successfully demonstrated reversible electrochemical insertion and removal in a Mg cathode using this strategy,[6] and this approach can also be used to study similar reactions for other cations (Li^+, Zn^{2+}, Mg^{2+}, Ca^{2+}) due to the stabilization of a specific host phase.

ACKNOWLEDGMENTS

This work was supported as part of the Joint Center for Energy Storage Research, an Energy Innovation Hub funded by the U.S. Department of Energy, Office of Science, Basic Energy Sciences. The Advanced Photon Source is supported by the DOE under Contract No. DE-AC02-06CH11357. This work made use of the Northwestern University Central Facilities supported by the Materials Research Science and Engineering Center (MRSEC) through National Science Foundation (NSF) under Contract No. DMR-1121262. The authors thank the beamline technical support from Christian M. Schlepuetz and Jenia Karapetrova at Sector-33, of APS. Authors thank Chunjoong Kim, Tanhong Yi, and Jordi Cabana from the University of Illinois at Chicago for helping synthesizing PLD target materials, Michael D. Biegalski for PLD growth support at Oak Ridge National Laboratory. The PLD preparation and characterization was conducted at the Center for Nanophase Materials Sciences, which is sponsored at Oak Ridge National Laboratory by the Scientific User Facilities Division, Office of Basic Energy Sciences, U.S. Department of Energy.

[1] F. Y. Cheng, J. A. Shen, B. Peng, Y. D. Pan, Z. L. Tao, and J. Chen, Nat. Chem. **3**, 79 (2011).

[2] J. P. Jacobs, A. Maltha, J. G. H. Reintjes, J. Drimal, V. Ponec, and H. H. Brongersma, J. Catal. **147**, 294 (1994).

[3] Y. Yamasaki, S. Miyasaka, Y. Kaneko, J. P. He, T. Arima, and Y. Tokura, Phys. Rev. Lett. **96**, 207204 (2006).

[4] Q. Song and Z. J. Zhang, J. Am. Chem. Soc. **126**, 6164 (2004).

[5] M. M. Thackeray, W. I. F. David, P. G. Bruce, and J. B. Goodenough, Mater. Res. Bull. **18**, 461 (1983).

[6] Z. Feng, X. Chen, L. Qiao, A. L. Lipson, T. T. Fister, L. Zeng, C. Kim, T. Yi, N. Sa, D. L. Proffit, A. K. Burrell, J. Cabana, B. J. Ingram, M. D. Biegalski, M. J. Bedzyk, and P. A. Fenter, ACS Appl. Mater. Interfaces **7**, 28438 (2015).

[7] C. Kim, P. J. Phillips, B. Key, T. Yi, D. Nordlund, Y.-S. Yu, R. D. Bayliss, S.-D. Han, M. He, Z. Zhang, A. K. Burrell, R. F. Klie, and J. Cabana, Adv. Mater. **27**, 3377 (2015).

[8] R. Vidu and P. Stroeve, Ind. Eng. Chem. Res. **43**, 3314 (2004).

[9] S. Mukerjee, T. R. Thurston, N. M. Jisrawi, X. Q. Yang, J. McBreen, M. L. Daroux, and X. K. Xing, J. Electrochem. Soc. **145**, 466 (1998).

[10] N. Kijima, T. Ikeda, K. Oikawa, F. Izumi, and Y. Yoshimura, J. Solid State Chem. **177**, 1258 (2004).

[11] W. H. Baur, Acta Crystallogr., Sect. B: Struct. Crystallogr. Cryst. Chem. **32**, 2200 (1976).

[12] D. B. Rogers, R. D. Shannon, and A. W. Sleight, Inorg. Chem. **8**, 841 (1969).

[13] C.-H. Kim, Z. Akase, L. Zhang, A. H. Heuer, A. E. Newman, and P. J. Hughes, J. Solid State Chem. **179**, 775–774 (2006).

[14] P. M. De Wolff, Acta Crystallogr. **12**, 341 (1959).

[15] J. E. Greedan, N. P. Raju, A. S. Wills, C. Morin, S. M. Shaw, and J. N. Reimers, Chem. Mater. **10**, 3058 (1998).

[16] R. Manaila and P. Pausescu, Phys. Status Solidi **9**, 385 (1965).

[17] M. Rosenberg and P. Nicolau, Phys. Status Solidi **6**, 101 (1964).

[18] L. Malavasi, C. Tealdi, M. Amboage, M. C. Mozzati, and G. Flor, Nucl. Instrum. Methods Phys. Res., Sect. B **238**, 171 (2005).

[19] D. Smith, *Thin-Film Deposition: Principles and Practice*, 1st ed. (McGraw-Hill Education, 1995).

[20] H. M. Christen and G. Eres, J. Phys.: Condens. Matter **20**, 264005 (2008).

[21] H. Jeen, W. S. Choi, M. D. Biegalski, C. M. Folkman, I. C. Tung, D. D. Fong, J. W. Freeland, D. Shin, H. Ohta, M. F. Chisholm, and H. N. Lee, Nat. Mater. **12**, 1057 (2013).

[22] R. G. Palgrave, P. Borisov, M. S. Dyer, S. R. C. McMitchell, G. R. Darling, J. B. Claridge, M. Batuk, H. Y. Tan, H. Tian, J. Verbeeck, J. Hadermann, and M. J. Rosseinsky, J. Am. Chem. Soc. **134**, 7700 (2012).

[23] See supplementary material at http://dx.doi.org/10.1063/1.4955135 for details on the pulsed laser deposition growth, X-ray characterization (including thin-film X-ray diffraction and X-ray reflectivity fitting results), atomic force microscopy and reflection high energy electron diffraction.

[24] K. S. Irani, A. P. B. Sinha, and A. B. Biswas, J. Phys. Chem. Solids **23**, 711 (1962).

[25] L. Malavasi, M. C. Mozzati, G. Chiodelli, C. B. Azzoni, and G. Flor, J. Mater. Sci. **39**, 1671 (2004).

[26] A. Yamada, J. Solid State Chem. **122**, 160 (1996).

[27] D. Santhanagopalan, D. Qian, T. McGilvray, Z. Y. Wang, F. Wang, F. Camino, J. Graetz, N. Dudney, and Y. S. Meng, J. Phys. Chem. Lett. **5**, 298 (2014).

[28] M. Liu, Z. Rong, R. Malik, P. Canepa, A. Jain, G. Ceder, and K. Persson, Energy Environ. Sci. **8**, 964 (2015).